Oscillatory zoning in crystal growth: A constitutional undercooling mechanism

Ivan L'Heureux
Nonlinear Dynamics Study Group and Ottawa-Carleton Institute for Physics, University of Ottawa, Ottawa, Ontario, Canada K1N 6N5
(Received 11 June 1993)

A simple isothermal constitutional mechanism is proposed to explain the oscillatory compositional zoning observed in many natural crystals. The model is based on the diffusion equation in an open system and realistic crystal-growth kinetics. A phenomenological partitioning coefficient K is introduced to relate the composition in the melt to the composition in the growing front. For concreteness, the model is applied to the plagioclase feldspar system, a geologically important solid-solution series. Growth rates are obtained from experimental growth data. A linear stability analysis of the model is presented. It is seen that for $K > 1$ the steady state is stable. It is possible, however, to define an effective partitioning coefficient which may be smaller than unity. In this case, the system may undergo a Hopf bifurcation and develop an oscillatory behavior. Direct numerical solutions indicate that oscillatory and chaotic zonings can indeed be obtained.

PACS number(s): 61.50.Cj, 05.70.Ln, 64.70.Dv, 05.45.+b

I. INTRODUCTION

In recent years, there has been much interest in pattern formation at the interface of a growing crystal such as dendritic, cellular, and skeletal textures [1]. A particularly simple type of pattern consists in oscillatory textures such as those occurring in many rapidly solidified alloys [2] or in the explosive crystallization of amorphous layers [3,4]. In these instances, the velocity of the growing front is typically very high ($\sim$ cm/s or larger).

In contrast, oscillatory growth pattern may occur under slow-solidification conditions for which the growth velocity is much smaller ($\sim\mu$m/s). The oscillatory zoning observed in many plagioclase feldspar crystals found in rocks of volcanic origin is one of the best known examples of such a pattern. Plagioclase minerals form a solid-solution series between a sodium-rich member, albite (Ab) $NaAlSi_3O_8$, and a calcium-rich term, anorthite (An) $CaAl_2Si_2O_8$. It has been known for a long time [5] that plagioclase feldspar crystal faces often exhibit more or less regular compositional variations as the distance changes from the core of the crystal to its rim. The variations have been studied using microprobes, laser interferometry or reflected-light differential interference contrast techniques [6]. Typically, the composition varies by 5–15 mole % and the periodicity is between 10 and 100 μm. Superposed to these small-scale variations, irregular and abrupt changes often occur. These abrupt variations may be related to corresponding changes in the physicochemical environment of the cooling medium. However, it is believed that the small-scale regular variations are the result of a self-organizing process inherent to the solidification mechanism and to the rock-forming conditions. Various other mineralogical systems also exhibit oscillatory zoning. It has been observed in volcanic rocks (augite [7] and olivine [8]), in metamorphic rocks [9], in garnets [10], in calcite ($CaCO_3$) grown from aqueous solutions [11], and in experimentally grown (Ba,Sr)SO_4 crystals [12].

Various growth models have been proposed to explain the origin of the oscillatory zoning in plagioclase feldspar. Brandeis, Jaupart, and Allègre [13] considered temperature-induced oscillations. Their model is based on a simplified one-dimensional heat equation with latent heat release at the crystal front and Newtonian cooling. A growth velocity which relaxes to the nonequilibrium kinetic value with some delay time is also used. They showed that solutions with an oscillatory character exist, but there are damped and do not form a limit cycle. The periodicity of the signal was also found to be of the order of centimeters, which is much larger than the length scale involved in oscillatory zoning. In fact, as the diffusion coefficient of the component in the melt is typically much smaller than the thermal diffusivity, it is believed that these oscillations are diffusion induced. Allègre, Provost, and Jaupart [14] considered a one-dimensional growth model based on the diffusion equation and a relaxation time between the actual growth velocity and its kinetic value. Linearizing about a slowly varying solution, they found an approximate transient solution which presents a damped oscillatory character. Haase *et al.* and Ortoleva [15] proposed a different model based on the diffusion equation and an autocatalytic geochemical reaction scheme with *ad hoc* assumptions for the rate constants. A similar model has been recently used by Wang and Merino [11] to explain the compositional variation of trace elements in calcite. A chemical limit cycle behavior is then obtained for the concentration. The basis for the validity of the *ad hoc* assumptions is, however, physically unclear. Lasaga [16] proposed a diffusion-based model together with a phenomenological partitioning coefficient $K = c_s/c$ relating the concentration of one component of interest in the solid c_s to its value c in the melt at the growing interface. He explicitly considered an equilibrium partitioning coefficient (which is larger than 1) and performed a direct numerical integration of the model. Using meaningful growth rate expressions, he did not find any oscillatory solution.

In this paper, a simple isothermal model is proposed to explain the oscillatory zoning observed in a binary mixture such as the plagioclase system. It is based on the diffusion equation with reasonable expressions for the growth rate. No relaxation time between the actual growth rate and its nonequilibrium kinetic expression is necessary, although it could easily be considered. The model is similar to the one in Ref. [16], except that nonequilibrium value of K are considered as well, with $K<1$. The possibility of a constant flow rate of material into and out of the cooling reservoir is also considered. We find that indeed limit cycle solutions do exist.

The physical origin of the oscillation is based upon the constitutional undercooling mechanism [17]. Constitutional undercooling occurs when the liquid in contact with the growing solid front has a composition different from its bulk value. This results in a concentration gradient in the vicinity of the front. The liquidus temperature at the front is then different from the liquidus temperature of the bulk equilibrium system. An effective isothermal undercooling is therefore induced. This degree of constitutional undercooling defines the intensity of the growth rate. The relative magnitude between the diffusion process and the growth in turn drives the change in concentration at the interface, which affects the degree of undercooling. The growth kinetics therefore provides the nonlinear feedback necessary for the existence of nontrivial asymptotic behavior.

More specifically, for the plagioclase feldspar system, we will see that the growth velocity is a strong increasing function of the melt interface concentration. This fact allows us to clarify the physical mechanism for oscillation in the following way. For $K>1$, crystal growth consumes solute so that the melt concentration is lower at the interface than far away from it. Suppose that a perturbation of the stationary concentration profile results in an increase of the interface concentration. The growth process will then proceed at a faster rate, thus leading to an increase in the consumption of solute, so that the melt interface concentration will have a tendency to decrease. The growth kinetics and the diffusion process have therefore stabilizing effects on the perturbation. One expects the stationary profile to be stable. For $K<1$, however, the situation is different. In this case, growth rejects more solute in the melt, so that the melt concentration is higher at the interface than far away from it. A perturbation of the stationary concentration profile which increases the melt interface will result in a still faster growth, which rejects more solute at the interface and increase its concentration further. The growth has therefore a destabilizing effect on the perturbation. This increase cannot go on forever, since at some point the concentration gradient will be so strong that the diffusion process will dominate and generate a tendency to reinstate the stationary profile. The same conclusion can be drawn if the initial perturbation lowers the interface stationary value. We see that the potential for oscillation and complex dynamical behaviors results from the fact that the nonequilibrium feedback growth process occurs at a faster rate as the interface concentration increases. These qualitative observations are indeed confirmed by our quantitative analysis.

The paper is divided as follows. In Sec. II, the basic equations defining the constitutional undercooling model are introduced. In order to relate this model to a realistic system, we specifically apply it to the plagioclase feldspar case. Growth rate expressions are needed for this purpose. In Sec. III, such semiempirical expressions are established from the laboratory measurements of Kirkpatrick *et al.* [18]. In Sec. IV, a stability analysis of the model is performed. The steady-state solution is first found. A formal expression for the concentration of the component of interest in the melt at the growing interface is then established in the form of an integral equation. A stability analysis is then performed. It is seen that for $K<1$, the system undergoes a supercritical Hopf bifurcation leading to the possibility of periodic asymptotic solutions. In Sec. V, we show typical numerical solutions indicating that periodic and chaotic solutions are indeed obtained beyond the Hopf bifurcation. We finally present some concluding remarks in Sec. VI. Two appendixes complete the analysis.

II. BASIC EQUATIONS

Since the observed compositional zoning fronts are often parallel, we consider here a simple one-dimensional model describing the isothermal crystal growth from a melt. We choose a frame of reference moving with the growing front in such a way that the origin $x=0$ is fixed at the front. The half-line $x>0$ corresponds to the melt. The position coordinate of the growing front in the laboratory frame is then $x'=x+\int_0^t V(t')dt'$, where $V(t)$ is the velocity of the front.

Let $c(x,t)$ be the concentration (number of moles per unit volume) of the component of interest in the melt. We consider the possibility that the melt reservoir is an open system with input feed of concentration $\hat{c}$ far from the growing front. In the absence of input feed, $\hat{c}$ is simply interpreted as the bulk concentration in the melt far from the growing front. The dynamical evolution of $c(x,t)$ is given by the diffusion equation

$$\frac{\partial c}{\partial t}=D\frac{\partial^2 c}{\partial x^2}+V\frac{\partial c}{\partial x}-\Gamma(c-\hat{c}) , \tag{2.1}$$

where D is the diffusion coefficient of the component in the melt. We neglect the concentration dependence of this coefficient. The last term on the right-hand side of Eq. (2.1) crudely describes the effect of the input feed. Γ corresponds to the input flow rate per unit volume and can be interpreted as the inverse of the average residence time of the component in the reservoir. This last term is analogous to the Newtonian cooling term in the heat equation.

The boundary condition far from the crystal-melt interface is such that the concentration is equal to the input feed concentration (or the bulk value in absence of input feed):

$$c(\infty,t)=\hat{c} . \tag{2.2}$$

The boundary condition at the growing front is derived from the continuity of the particle current at the inter-

face:

$$D\frac{\partial c}{\partial x}\bigg|_0+[c(0,t)-c_s(0,t)]V=0 \ . \tag{2.3}$$

Here $c_s(0,t)$ and $c(0,t)$ are the interface concentration of the component in the crystal and in the melt, respectively. We have neglected the diffusion in the solid phase. In order to solve the diffusion equation, a relation between $c_s(0,t)$ and $c(0,t)$ is needed. Although various phenomenological relations may be used [19], the simplest one is established by introducing a constant partitioning coefficient K [16]:

$$c_s(0,t)=Kc(0,t) \ . \tag{2.4}$$

This phenomenological relation is approximately valid when c refers to the concentration of a trace component. The boundary condition at the interface then becomes

$$D\frac{\partial c}{\partial x}\bigg|_0+c(0,t)(1-K)V=0 \ . \tag{2.5}$$

In the case where c refers to a major component, other phenomenological relations can be used [16]. For instance, for a two-component system, the partitioning coefficient can be interpreted in terms of an exchange equilibrium constant K_D:

$$K_D=\frac{c_s(0,t)c'(0,t)}{c(0,t)c_s'(0,t)} \ , \tag{2.6}$$

where $c_s'(0,t), c'(0,t)$ denote the interface concentration of the other solid-solution component in the crystal and in the melt, respectively. Using the mass balance equations to eliminate $c'(0,t)$ and $c_s'(0,t)$, it can be shown [16] that

$$c_s(0,t)=\frac{K_DBc(0,t)}{A+(K_D-1)c(0,t)} \ , \tag{2.7}$$

where A,B are approximately constant. If the concentration $c(0,t)$ does not change very much in time, one can still define [16] an effective partitioning coefficient

$$K=\frac{K_DB}{A+(K_D-1)\langle c(0,t)\rangle} \ , \tag{2.8}$$

where $\langle c(0,t)\rangle$ denotes the time average of the concentration. One then approximately recovers the boundary condition (2.4).

Finally, we choose the initial condition to be such that the concentration is equal to the input feed concentration (or its bulk value in absence of feed):

$$c(x,0)=\hat{c} \ . \tag{2.9}$$

In order to complete the description of the model, we need to specify the speed of the growing front. This provides the nonlinear coupling necessary to generate self-oscillatory solutions. As the growing process is typically slow, we assume that the speed of the growing front relaxes instantaneously to its value $G_T(c(0,t))$ defined by growth kinetic models at temperature T:

$$V(t)=G_T(c(0,t)) \ . \tag{2.10}$$

Equations (2.1)–(2.4), (2.9), and (2.10) define the model considered here. The control parameters are then D, Γ, T, $\hat{c}$, and K.

III. GROWTH RATE

In order to apply the model to a realistic natural system, we need to find an explicit expression for the growth rate G_T. For concreteness, we choose the plagioclase feldspar Ab-An system as example. Indeed, since it constitutes a system of prime importance in geological conditions, its thermodynamics and growth rate kinetics have been carefully studied [18,20,21]. In this section, we propose to derive semiempirical expressions for the growth rate of plagioclase feldspar based on the laboratory measurements of Kirkpatrick *et al.* [18]. Our approach is similar to the one used elsewhere [16,22], but does not necessitate the use of viscosity data.

We have found that a good fit to the data is given by the Calvert-Uhlmann model [23] for the growth of large crystals. This model expresses the overall growth rate as a geometric average of two processes: a longitudinal growth R_s by surface nucleation and a continuous growth R_c responsible for the lateral spread of the crystal:

$$G_T=U(R_SR_C^2)^{1/3} \ , \tag{3.1}$$

where

$$R_S=\exp(-3a/T\Delta T)\exp[-b/(T-T_g)] \ , \tag{3.2}$$

$$R_C=[1-\exp(-\Delta G/RT)]\exp[-b/(T-T_g)] \ . \tag{3.3}$$

Here U is a velocity scale, a depends on the surface tension of the two-dimensional nuclei generating the longitudinal growth, and b is proportional to the activation enthalpy for the transport of atomic movement through the liquid and across the interface and is related to the viscosity of the melt. ΔT is the undercooling

$$\Delta T=T_L-T \ , \tag{3.4}$$

where T_L is the equilibrium liquidus temperature. T_g in the term $\exp[-b/(T-T_g)]$ denotes the glass transition temperature. A slightly better fit was obtained with this term rather than the more conventional one $\exp(-b/T)$, reflecting the validity of the Vogel-Tammann-Fulcher empirical relation [24] describing the temperature dependence of the viscosity in many liquids. In Eq. (3.3), R is the ideal gas constant and $\Delta G>0$ denotes the molar Gibbs free-energy difference between the crystal and the liquid. For not too large undercooling, this quantity is conventionally related to ΔT through the relation

$$\Delta G=\Delta H\Delta T/T_L \ , \tag{3.5}$$

where ΔH is the enthalpy difference between the crystal and the liquid. This quantity in turn can be expressed as

$$\Delta H=\Delta H_f+\Delta H_m \ , \tag{3.6}$$

where the first term on the right-hand side represents the

molar enthalpy of fusion and the second term the molar enthalpy of mixing.

A relation between the growth velocity and the concentration is needed. Using the empirical data of Ref. [18], we have fitted the three parameters $\ln U, a, b$ to quadratic polynomials in X, the An composition (mole fraction) in the melt:

$$\ln U(X)=\sum_{n=0}^{2} u_n X^n , \tag{3.7}$$

$$a(X)=\sum_{n=0}^{2} a_n X^n , \tag{3.8}$$

$$b(X)=\sum_{n=0}^{2} b_n X^n . \tag{3.9}$$

Table I gives the list of coefficients u_n, a_n, b_n. We adopt Lasaga's fitting polynomial [16] for the liquidus curve T_L (in K):

$$T_L = 1392.5 + 1610.01X - 3219.3X^2 + 3235.2X^3 - 1187.6X^4 . \tag{3.10}$$

The glass transition temperature (in K) is taken from [20]

$$T_g = 1085X + (1-X)1018 . \tag{3.11}$$

Using Ref. [20], we take the enthalpies of fusion and mixing (in cal/mole) to be:

$$\Delta H_f = 23.99T_L - 6.95\times 10^{-3}T_L^2 - \frac{15.01\times 10^5}{T_L} - 3224 , \tag{3.12}$$

$$\Delta H_m = -X(1-X)(6667 - 15X + 3893X^2) . \tag{3.13}$$

Finally, the relation between the concentration $c(0,t)$ of An and the composition X in the melt at the interface is

$$c(0,t)=\frac{X}{v_{\mathrm{An}}X + (1-X)v_{\mathrm{Ab}}} , \tag{3.14}$$

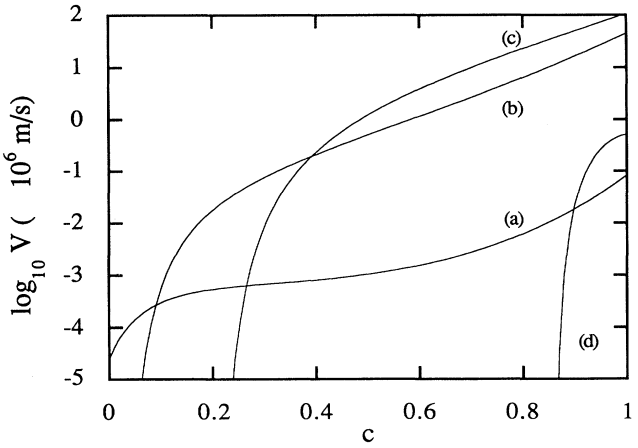

FIG. 1. Behavior of the growth velocity $V=G_T$ with c, the An concentration in units of inverse molar volume for various temperatures. (a) $T=1200$ K; (b) $T=1400$ K; (c) $T=1600$ K; (d) $T=1800$ K.

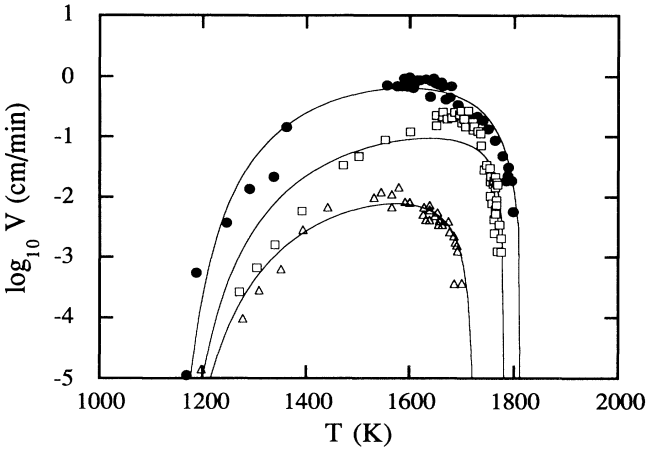

FIG. 2. Comparison of the calculated growth velocity curves and the empirical data of Ref. [18] for various An melt concentrations: $c=1.0$ (circles); $c=0.75$ (squares); $c=0.50$ (triangles).

where $v_{\mathrm{An}}, v_{\mathrm{Ab}}$ are the molar volume of An and Ab, respectively. It turns out that these two molar volumes are nearly equal ($v_{\mathrm{An}}=100.79$ cm^3/mole, $v_{\mathrm{Ab}}=100.07$ cm^3/mole), so that, to a good approximation,

$$c(0,t)=X/v_{\mathrm{An}} . \tag{3.15}$$

Measuring the concentration of An in units of inverse molar volume, we see that the composition X gives directly the concentration $c(0,t)$.

Equations (3.1)–(3.13) and (3.15) define in our model the growth velocity G_T as a function of c at temperature T. Figure 1 shows the behavior of the growth velocity as a function of the concentration for various temperatures. In Fig. 2, the growth velocity curves are compared with the empirical data of Kirkpatrick *et al.* [18]. The fits are reasonably good for a large range of temperatures and concentrations. It should be noted that the low-concentration data ($X=0.20$) of Kirkpatrick *et al.* are significantly different from the theoretical prediction. In view of the fact that the corresponding sample was treated differently from the others [22], these data were in fact not considered when obtaining the fitting parameters of Table I. Recent measurements of growth velocity at low An concentrations [22] are indeed consistent with our theoretical curves.

It turns out that the main terms defining the shape of the growth curve as a function of c are the velocity scale dependence $U(X)$ and the liquidus temperature $T_L(X)$. The growth curves depends only slightly on the other terms $a(X)$, $b(X)$, $T_g(X)$, $\Delta H_f(X)$, and $\Delta H_m(X)$.

TABLE I. Coefficients of the polynomials defined in Eqs. (3.7)–(3.9) as determined from the data of Kirkpatrick *et al.* [18]. In (3.7)–(3.9), U is measured in cm/min, a is in K^2, and b in K.

n	u_n	a_n	b_n
0	−4.0204	1 225 890	1099.6
1	7.1197	−3 509 543	2193
2	0	2 566 582	−2114.3

IV. LINEAR ANALYSIS

A. Steady-state solution

The steady-state solution of the model can be obtained by setting the left-hand side of Eq. (2.1) equal to 0. The growth rate is then constant $V=V_0$. The time-independent solution of Eq. (2.1) satisfying the boundary conditions (2.2) and (2.5) is then

$$c_0(x)=\hat{c}\left[1+\frac{2(1-K)}{2K-1+\alpha}\exp[-V_0(1+\alpha)x/2D]\right], \tag{4.1}$$

where

$$\alpha=\left[1+\frac{4\Gamma D}{V_0^2}\right]^{1/2}. \tag{4.2}$$

The melt steady-state concentration at the interface $c_0\equiv c_0(x=0)$ is then

$$c_0=\hat{c}\frac{(1+\alpha)}{2K+\alpha-1}. \tag{4.3}$$

The relation between the steady-state growth rate V_0 and c_0 is consequently

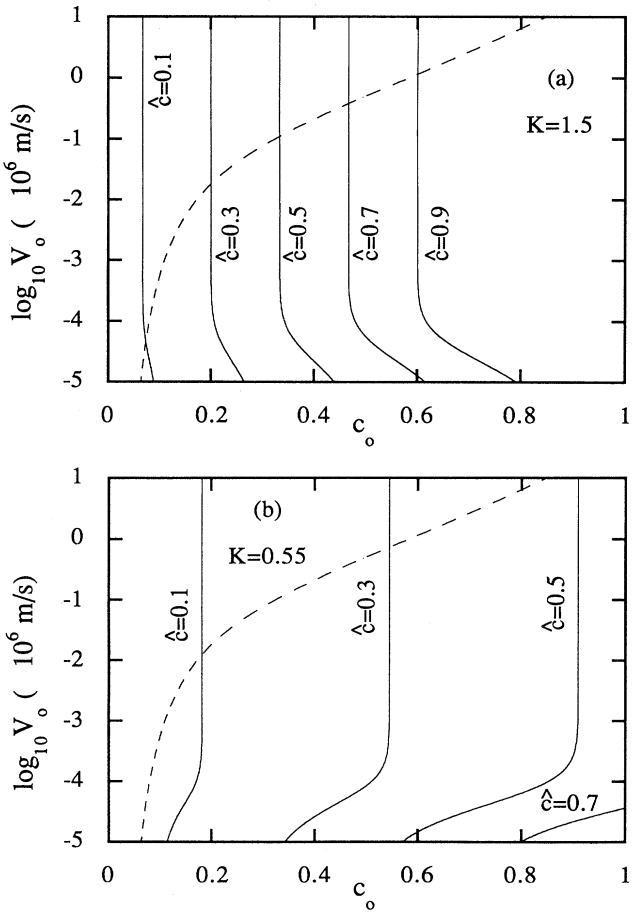

FIG. 3. Plots of the relationship between the steady-state growth velocity and the steady-state concentration according to Eq. (4.4), for various $\hat{c}$. The growth velocity curve of Fig. 1 for $T=1400$ K is superposed to the plots. (a) $K=1.5$; (b) $K=0.55$.

$$V_0=2\sqrt{\Gamma D}\left\{\left[1-2K+2\frac{(1-K)\hat{c}}{c_0-\hat{c}}\right]^2-1\right\}^{-1/2}, \tag{4.4}$$

where the quantity in square brackets is restricted to be positive. In the absence of input feed ($\Gamma=0$) the solution reduces to $c_0=\hat{c}/K$, in agreement with the solution of the constant velocity problem obtained by Smith, Tiller, and Rutter [25].

In the following, we can choose the diffusion coefficient D of the various elements in a typical silicate melt between 10^{-11} and 10^{-10} m^2/s. The value of Γ, the inverse average residence time, may be estimated [26] at 10^{-11} s^{-1}. Finally, although the partitioning coefficient K has an equilibrium value that is larger than 1, it is possible [19,27] to consider an effective K that is smaller than 1 in view of the approximate interpretation given by Eq. (2.8).

The function (4.4) is plotted in Fig. 3 for various values of $\hat{c}$. A typical ($T=1400$ K) growth rate curve $V=G_T$ is superposed showing the position of the steady-state solution. In most cases, the steady state solution is unique. However, for $K<1$ it is possible to find values of T and $\hat{c}$ for which there exist up to three different steady states for a small range of parameter values.

B. Time-dependent solution

In this section, we obtain the formal solution $c(x,t)$ of the time-dependent problem, given $V(t)$. An expression for the concentration c at the interface is then derived. We first take the spatial Laplace transform of Eq. (2.1) and take the boundary conditions (2.2) and (2.5) and the initial condition (2.9) into account. We get

$$\frac{d\bar{c}}{dt}=-[V(t)K+sD]c(0,t)+[s^2D+sV(t)-\Gamma]\bar{c}+\Gamma\hat{c}/s, \tag{4.5}$$

where $\bar{c}(s,t)=\int_0^\infty c(x,t)\exp(-sx)dx$ is the Laplace transform. The solution is then

$$\begin{aligned}\bar{c}(s,t)=&\frac{\hat{c}}{s}\exp p(t,0)\\&-\int_0^t dt'c(0,t')[sD+KV(t')]\exp p(t,t')\\&+\int_0^t dt'\frac{\Gamma\hat{c}}{s}\exp p(t,t'),\end{aligned} \tag{4.6}$$

where the propagator is

$$p(t,t')=s^2D(t-t')+sf(t')-\Gamma(t-t') \tag{4.7}$$

and

$$f(t')\equiv\int_{t'}^t V(t'')dt'' \tag{4.8}$$

is the length of the crystal growth between times t' and t. Performing a Laplace inversion finally gives the time- and space-dependent concentration. We obtain after some algebra

$$\begin{aligned}c(x,t)=&\hat{c}-\int_0^t dt'\frac{\hat{c}}{2}g_{t,t'}(x)\left[\frac{x+f(t')}{t-t'}-2V(t')\right]\\&+\int_0^t dt'\frac{c(0,t')}{2}\\&\times g_{t,t'}(x)\left[\frac{x+f(t')}{t-t'}-2KV(t')\right],\end{aligned} \tag{4.9}$$

where

$$g_{t,t'}(x)=\frac{\exp\left[-\Gamma(t-t')-\dfrac{[x+f(t')]^2}{4D(t-t')}\right]}{[4\pi D(t-t')]^{1/2}} . \quad (4.10)$$

The concentration at the interface is given by taking the limit $x\to 0$. However, a careful asymptotic analysis is needed as this limit is not well defined when $t\to t'$ in the integral. An outline of the analysis is found in Appendix A. We finally obtain

$$c(t)\equiv c(0,t)=\hat{c}-\int_0^t dt'\hat{c}g_{t,t'}(0)\left[\frac{f(t')}{t-t'}-2V(t')\right] + \int_0^t dt'c(t')g_{t,t'}(0)\left[\frac{f(t')}{t-t'}-2KV(t')\right] . \quad (4.11)$$

It is easily verified that taking the large time limit of this solution and setting $c(t')$ constant, one recovers the steady-state solution (4.3).

C. Stability analysis

We now investigate the linear stability of the steady-state solution obtained in Sec. IV B by considering the time behavior of a small perturbation of V and c about the steady state. As usual, we let a solution of the form

$$c=c_0+\epsilon e^{2\omega t/\tau_m} , \quad (4.12)$$

$$V=V_0+\epsilon V' e^{2\omega t/\tau_m} , \quad (4.13)$$

where ϵ is the amplitude of the small perturbation and V' is the derivative of the growth curve with respect to c evaluated at the steady state. Here, τ_m is a natural time scale

$$\tau_m=\frac{8D}{V_0^2\alpha^2} , \quad (4.14)$$

with α defined in Eq. (4.2) and ω is the dimensionless eigenvalue of the linearized problem.

The stability analysis is similar to the one considered by Van Saarloos and Weeks [3] and is outlined in Appendix B. We find that the eigenvalue ω obeys the relation

$$\sqrt{\omega+1}=\frac{\omega Q-P}{\omega-P} , \quad (4.15)$$

where

$$P=-4\theta\frac{(\alpha+1)(1-K)}{\alpha^2(\alpha-1+2K)} , \quad (4.16)$$

$$Q=\frac{1-2K}{\alpha}+2\theta\frac{(\alpha+1)(1-K)}{\alpha(\alpha-1+2K)} . \quad (4.17)$$

Here

$$\theta=\hat{c}V'/V_0 \quad (4.18)$$

is the dimensionless slope of the growth curve at the steady state and is positive for the An-Ab system. The solution of (4.15) is also a solution of

$$\omega^2+\omega(1-2P-Q^2)+(P^2-2P+2QP)=0 \quad (4.19)$$

so that the stability analysis is straightforward. The two solutions $\omega_\pm$ of (4.19) are

$$\omega_\pm=-\tfrac{1}{2}(1-2P-Q^2)\pm\tfrac{1}{2}|Q-1|\sqrt{(1+Q)^2+4P} . \quad (4.20)$$

However, it must be verified that the solutions $\omega_\pm$ of (4.19) indeed solve (4.15).

For $K>1$, it is seen that $P>0$ since $\theta>0$. In this case, the roots $\omega_\pm$ are both real. For these roots to be a solution of (4.15), it is required that the right-hand side of (4.15) be positive, which simplifies to

$$-\tfrac{1}{2}[1-Q\pm\sqrt{(1+Q)^2+4P}]>0 . \quad (4.21)$$

Since $Q<0$ for $K>1$, it is seen that ω_+ is never a solution of (4.15) while ω_- exists for $1-Q>\sqrt{(1+Q)^2+4P}$, which is equivalent to

$$\theta>\frac{\alpha(2K-1)(\alpha-1+2K)}{2(2-\alpha)(\alpha+1)(K-1)} . \quad (4.22)$$

It is also easy to verify that in this domain of existence, ω_- is always <0, so that the steady-state solution is stable.

For $K<1$, the situation is different for then $P<0$ and Q may be positive. The case where $\omega_\pm$ are real $[(1+Q)^2+4P>0]$ is first considered. For the sake of argument, we examine the range $\frac{1}{2}<K<1$. When $Q<1$, we find the same result as for the case $K>1$: ω_+ is not a solution of (4.15) while ω_- solves it when the inequality (4.22) is obeyed. ω_- is also negative in this domain so that the steady state is stable. When $Q>1$ [and $(1+Q)^2+4P>0$], it is found from (4.21) that ω_+ is always a solution of (4.15) while ω_- has this property when

$$\theta<\frac{\alpha(2K-1)(\alpha-1+2K)}{2(2-\alpha)(\alpha+1)(K-1)} . \quad (4.23)$$

The sign of $\omega_\pm$ and the stability of the steady state depends on the relative magnitude of the two terms in the right-hand side of Eq. (4.20). Similar observations apply when $K<\frac{1}{2}$, except that the inequality sign is reversed in (4.22) and (4.23).

The most interesting case occurs for $(1+Q)^2+4P<0$ since the roots $\omega_\pm$ becomes complex. In this case, both $\omega_\pm$ are solution of (4.15) when $Q>1$. This last condition is equivalent to

$$\theta>\frac{(\alpha-1+2K)^2}{2(\alpha+1)(1-K)} . \quad (4.24)$$

The sign of $\mathrm{Re}(\omega_\pm)$ determines the nature and the stability of the steady state. When $1-2P-Q^2>0$ the steady state is stable and the approach to it has an oscillatory behavior. However, for $1-2P-Q^2<0$, the steady state is unstable and the system exhibits a supercritical Hopf bifurcation at the critical line

$$1-2P-Q^2=0 , \quad Q>1 \qquad (1+Q)^2+4P<0 . \quad (4.25)$$

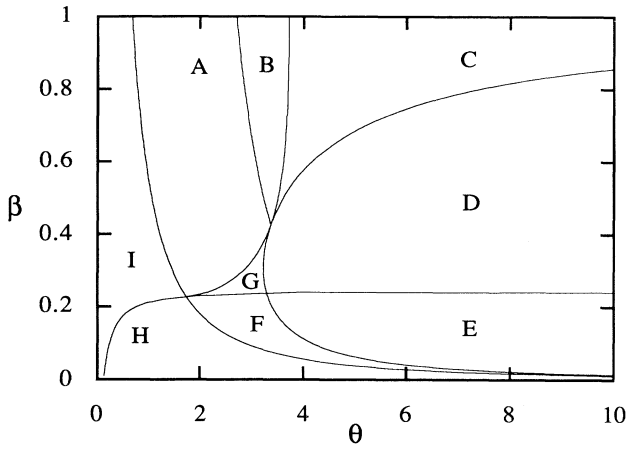

FIG. 4. Phase diagram exhibiting the behavior of the steady state according to a linear stability analysis for $K=0.55$. The parameters (θ,β) are defined in Eqs. (4.18) and (4.26). In regions A and B, $\mathrm{Im}\omega_{\pm}>0$ with $\mathrm{Re}\omega_{\pm}<0$ (region A) and $\mathrm{Re}\omega_{\pm}>0$ (region B). In the other regions, the eigenvalues (when they exist) are real. C, $\omega_{\pm}>0$; D, $\omega_{\pm}>0$ and $\omega_{-}<0$; E, $\omega_{+}>0$ is the only root of (4.15); F, $\omega_{+}<0$ is the only root of (4.15); G, $\omega_{\pm}<0$; H, $\omega_{-}<0$ is the only root of (4.15); I, no solution for (4.15).

A self-oscillatory solution is then possible beyond the bifurcation.

In Fig. 4, a complete typical stability diagram is illustrated for $K<1$. This phase diagram is shown in terms of the dimensionless slope of the growth curve θ and a parameter related to the inverse average residence time

$$\beta\equiv 1/\alpha^2=1/(1+4\Gamma D/V_0^2)\ , \tag{4.26}$$

with $0<\beta\leq 1$. The region where $\omega_{\pm}$ complex solve (4.15) with $\mathrm{Re}(\omega_{\pm})>0$ is rather small, but, as we will see in the next section, it is accessible in realistic conditions.

V. NUMERICAL SOLUTION

In order to verify the findings of the preceding section and to investigate the nature of the linearly unstable solutions, a direct numerical solution of the evolution equation (2.1) was obtained.

We rewrite Eq. (2.1) in nondimensional form by scaling distance by D/V_0 and time by D/V_0^2. The velocity scale is then V_0. We discretize the space and time variables using a fixed space and time steps Δx and Δt on staggered grids $x=j\Delta x, t=n\Delta t$. The dimension M of the spatial grid is chosen large enough (in practice $M\Delta x=5$). A semi-implicit scheme is adopted for the time evolution and centered differences are used to approximate the spatial derivatives. The discretized version of the evolution equation (2.1) and of the boundary conditions transform the differential equation into a nonlinear matrix equation of the form

$$\mathbf{A}(c_0^{n+1})\mathbf{C}^{n+1}=\mathbf{B}(\mathbf{C}^n)\ , \tag{5.1}$$

where the jth element of $\mathbf{C}^n$ is the concentration c_j^n at time n and space label j, $\mathbf{A}$ is an $M\times M$ matrix, and $\mathbf{B}$ is a column vector. The nonlinear dependence of $\mathbf{A}$ on c_0^{n+1} is due to the coupling of the concentration field to the velocity of the growing front. The inversion of (5.1) is performed by starting from an initial guess for $\mathbf{C}^{n+1}$ in $\mathbf{A}$ and inverting. Let $R_j\equiv\sum_j A_{ij}c_j^{n+1}-B_i$ be the residue. The inversion is iterated until the quantity

$$\left[\frac{\sum_j (R_j)^2}{\sum_j (c_j^{n+1})^2}\right]^{1/2}$$

is smaller than a tolerance δ. In order to exercise a better control on the speed of convergence [28], a relaxation factor γ is introduced:

$$\mathbf{C}^{n+1,i+1}=\gamma\mathbf{C}^{n+1,i+1}+(1-\gamma)\mathbf{C}^{n+1,i}\ , \tag{5.2}$$

where i denotes the iteration index. The numerical algorithm was checked for convergence and stability. As a further verification, the numerical solution for the linear problem $V=\text{const}$ and $\Gamma=0$ agreed with the known analytical solution [25]:

$$c=\frac{\hat{c}}{2K}\left(1+\mathrm{erf}\left(\sqrt{V^2t/4D}\right)-(1-2K)e^{-K(1-K)V^2t/D}\times\left\{1+\mathrm{erf}\left[(1-2K)\sqrt{V^2t/4D}\right]\right\}\right)\ . \tag{5.3}$$

Figure 5 gives typical plots of the concentration of An in the solid $c_s(t)=Kc(t)$ as a function of the distance $x=\int_0^t V(t')dt'$ from the core of the crystal for various parameter values. In practice, we chose $\Delta x=0.05$, $\Delta t=0.005$, $M=100$, $\delta=1.0\times10^{-6}$, and $\gamma=0.5$.

Figure 5(a) corresponds to $K>1$. The solution approaches the (stable) steady state without oscillation, in accordance with the stability analysis of Sec. IV.

In Figs. 5(b)–5(d), the partitioning constant is chosen smaller than 1 and $\hat{c}$ is varied. The plot of Fig. 5(b) corresponds to a point in region A of the phase diagram of Fig. 4. As expected from the stability analysis, the solution has an oscillatory character and approaches the stable steady state.

Figures 5(c) and 5(d) correspond to points in region B of the phase diagram, where the steady state is unstable and the eigenvalues of the linearized problem possess a nonzero imaginary part. In Fig. 5(c), the system is located just beyond the Hopf bifurcation where a periodic solution is expected. This is indeed the case. The distance between the peaks in the signal is $5.41D/V_0$. In view of the fact that V_0 is insensitive to the value of D in the range of interest, this spatial periodicity corresponds to 47–470 μm for $D=10^{-11}$–10^{-10} m^2/s, respectively. This value is consistent with typical observations of compositional zoning in natural plagioclases, particularly for the lower values of D.

Finally, in Fig. 5(d) the parameter $\hat{c}$ is further increased with respect to the value in Fig. 5(c). However, the system is still in region B of Fig. 4. The numerical algorithm shows that the solution has developed an irregular chaotic character.

Because of the small magnitude of Γ, the fact that the system is open has little effect on the solution curves of Fig. 5: for all these, $\beta=1/(1+4\Gamma D/V_0^2)$ is very close to 1. It is only for small values of $\hat{c}$ that the system typically moves towards the lower right corner of the phase diagram of Fig. 4. For such values of the parameters, the steady state is unstable, but the numerical solution indicated that the system quickly stops growing [$V(t)\rightarrow 0$]. It should be noted that in many instances, the peak values of the numerically obtained melt concentration was sometimes slightly higher than 1 [this is not the case for Fig. 5(c)]. This is not surprising in view of the fact that there are no terms in the expression for the growth rate which formally constraint c to be less than 1. This problem should not arise with a more exact expression for the growth rate.

VI. CONCLUSION

In this paper, we have studied a simple isothermal constitutional undercooling model giving the concentration of one component of a two-species binary mixture at the position of the crystallization front. The model is based on the conservation of mass (diffusion equation) together with reasonable growth kinetics. The possibility of a continuous flow of matter with the outside was also considered by introducing an inverse average residence time Γ. The model has been applied to a geologically important natural system known to exhibit in many instances a complex or oscillatory compositional zoning: the anorthite-albite solid solution series.

A complete linear stability analysis of the steady state has been presented. It has been shown that when the effective or equilibrium partitioning coefficient is larger than unity, the steady state is stable. This fact explains why Lasaga [16] was not able to obtain oscillatory numerical solutions. However, when the effective partitioning coefficient is smaller than unity, there exist regions in the control parameters space for which the steady state is unstable and develops an oscillatory character.

Direct numerical solutions have been obtained and we indeed established the presence of self-oscillatory solution

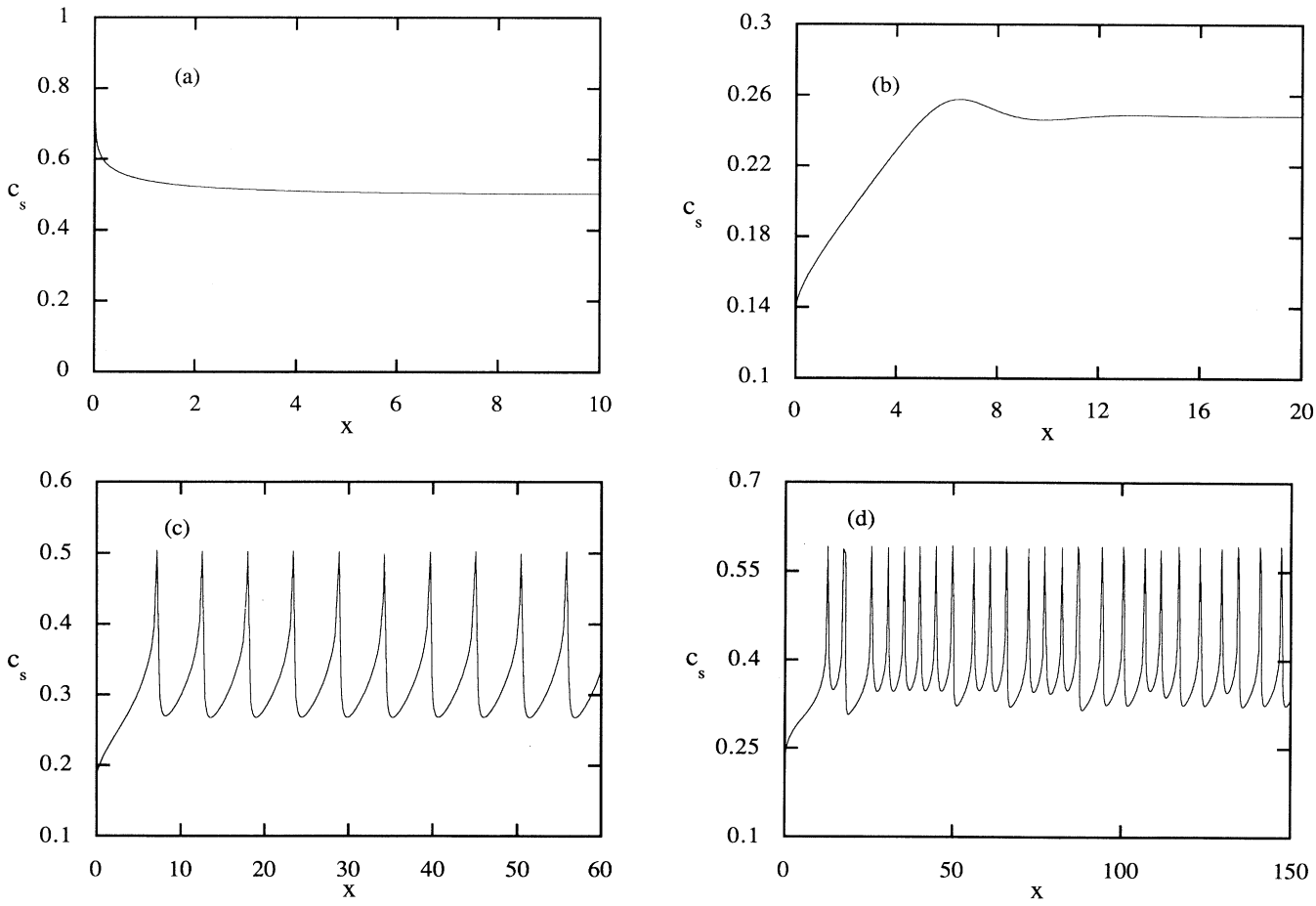

FIG. 5. Numerical solution of the concentration of An in the crystal at the growing front as a function of the distance from the core $x=\int_0^t V(t')dt'$ (in units of D/V_0). The parameters are $D=10^{-10}$ m^2/s, $\Gamma=10^{-11}$ s^{-1}, and $T=1400$ K. (a) $K=1.5$, $\hat{c}=0.5$ ($V_0=0.1107$ μm/s, initial undercooling $\Delta T=322.8$ K); (b) $K=0.55$, $\hat{c}=0.25$ ($V_0=0.3411$ μm/s, initial undercooling $\Delta T=239.7$ K); (c) $K=0.55$, $\hat{c}=0.33$ ($V_0=1.1577$ μm/s, initial undercooling $\Delta T=275.4$ K); (d) $K=0.55$, $\hat{c}=0.415$ ($V_0=4.3133$ μm/s, initial undercooling $\Delta T=302.2$ K).

with a periodicity compatible with the observations. Irregular (chaotic) solutions were also obtained by varying the bulk concentration $\hat{c}$, thereby increasing the initial undercooling. In contrast to the explosive crystallization problem [3], no clear period doubling cascade was found. The transition from an oscillatory solution to chaos needs to be further investigated. Because the value of the inverse average residence time Γ in the system in consideration is small, its effect was seen to be negligible. Consequently, our observations apply for a closed system as well.

Generalizations of our basic model to reflect more realistic conditions are currently under investigation. For instance, the more appropriate boundary condition (2.7) should be considered instead of (2.4). The case of an equilibrium concentration-dependent partitioning coefficient $K(c)$ as defined by the ratio of the solidus and the liquidus curves could also be investigated. Also, an explicit time dependence in the temperature of the reservoir or in the bulk concentration $\hat{c}$ could be considered. When these parametric variations are sufficiently slow, one expects a drift of the steady-state concentration in time. This could translate into a drift of the extrema of the oscillatory signal. This drift is in fact observed in many instances of natural plagioclases [6].

A relaxation time $\mathcal{T}$ between the actual growth rate and its nonequilibrium kinetic value G_T may also be considered as in previous models [13,14]. Specifically, the growth rate relation (2.10) is replaced by

$$\mathcal{T}\frac{dV}{dt}+V=G_T \ . \tag{6.1}$$

The stability eigenvalue equation (4.15) is then replaced by

$$\sqrt{\omega+1}=\frac{\omega Q-P+\dfrac{2(1-2K)\mathcal{T}}{\alpha\tau_m}\omega^2}{\omega-P+2\mathcal{T}\tau_m^{-1}\omega^2} \ . \tag{6.2}$$

A detailed analysis is beyond the scope of this paper. Nevertheless, it can be verified that no complex eigenvalues with positive real part were found for $K>1$, indicating that the presence of the relaxation time $\mathcal{T}$ is not sufficient to induce a limit cycle behavior. In agreement with the findings of Allègre, Provost, and Jaupart [14], the steady state is stable, although damped oscillations are possible.

In many open complex systems, uncontrollable fluctuations of the environmental factors may be modeled as a random variation of the external parameters $D,\Gamma,T,\hat{c},K$. The stochastic character of the dynamical system may lead to a large variety of nontrivial behaviors [29]. The question of such noise-induced transitions in our model is a relevant one and is presently under study.

In conclusion, our simple model can qualitatively explain with few assumptions the compositional zoning profile observed in various natural systems. An understanding of the mechanism generating oscillatory zoning allows us to clarify the circumstances in which many crystals in nature have been formed and to get relevant information on the rock-forming conditions.

Note added in proof. The expression (3.10) for the heat of fusion pertains to pure Ab extrapolated on the liquidus curve. One may argue that more reasonable expressions for ΔH_f should be used, such as an average of the heat of fusion of pure An and pure Ab weighted by the composition. However, the growth curves are not sensitive to the particular value of ΔH_f chosen within reasonable bounds. In fact, using such a new expression for ΔH_f leads to results which are essentially identical.

ACKNOWLEDGMENTS

This research was supported by a grant from the Natural Sciences and Engineering Research Council of Canada. The author wishes to thank Tony Fowler for fruitful discussions about the fascinating nonequilibrium patterns found in geological systems and careful reading of the manuscript. Finally, I would like to thank Godelieve Deblonde for helpful comments on the numerical method used here.

APPENDIX A

In this appendix, the asymptotic evaluation of the limit $x\to 0$ in Eq. (4.9) is outlined, leading to Eq. (4.11). This evaluation is inspired from a similar calculation of Lasaga, Richardson, and Holland [30]. In the time integrals of Eq. (4.9), we change variables to $u=1/[2(t-t')^{1/2}]$. The integration limits are changed from $(0,t)$ to $[1/(2\sqrt{t}),\infty]$. The argument of the exponential in the integrals become $-(u^2/D)\{x+f[t-1/(4u^2)]\}^2-\Gamma/(4u^2)$. An auxiliary large parameter v is chosen $1/(2\sqrt{t})<v<\infty$, thus splitting the integrals into two parts.

In the first part of the integrals $1/(2\sqrt{t})<u<v$, one can set $x=0$ in the integrand. Transforming back to the original time variable t', this first part of the integrals becomes a time integral from 0 to $t-(1/4v^2)$ of the integrand function evaluated at $x=0$. Finally, since v is large, the term $1/(4v^2)$ may be neglected compared to t in the upper limit.

In the second part of the integrals, the limits are $v<u<\infty$. Since v is large, u is also large (i.e., t is close to t'). The function $f(t)$ is then arbitrary close to zero. We neglect $f(t)$ compared to x. Taking the limit of large u, it is easy to see that the second part of the integrals reduce to

$$-\frac{\hat{c}-c(t)}{\sqrt{\pi D}}\int_y^\infty du\, xe^{-u^2x^2/D}=[c(t)-\hat{c}]/2 \ .$$

The equality results from taking the limit $x\to 0$ after the integral is evaluated. Collecting the result, we finally obtain Eq. (4.11).

APPENDIX B

In this appendix, we outline the derivation of the eigenvalue equation (4.15) starting from the ansatz (4.12) and (4.13). The approach is similar to the one used by Van Saarloos and Weeks [3]. In Eq. (4.11), it is convenient to introduce $\tau=t-t'$. Changing the variable of integration from τ to f defined in (4.8), one can write Eq. (4.11) as

$$c(t)=\hat{c}+2\hat{c}\int_0^L \frac{df}{\sqrt{4\pi D\tau}} e^{-\Gamma\tau-f^2/4D\tau} - 2K\int_0^L c(t-\tau)\frac{df}{\sqrt{4\pi D\tau}} e^{-\Gamma\tau-f^2/4D\tau} + \int_0^L df[c(t-\tau)-\hat{c}]\frac{f}{\tau V(t-\tau)\sqrt{4\pi D\tau}} \times e^{-\Gamma\tau-f^2/4D\tau} . \quad \text{(B1)}$$

Here $L\equiv f(0)$ is the total length of the crystal. $\tau(f,t)$ is then implicitly given by the definition (4.8) of f:

$$f(t-\tau)=\int_{t-\tau}^{t} V(t'')dt'' . \quad \text{(B2)}$$

We define τ_0 by $f(t-\tau)\equiv\tau_0 V_0$. Substituting (4.13) into (B2), one finds the first-order correction $\delta\tau$ due to the perturbation:

$$\delta\tau=\tau-\tau_0=-\frac{\epsilon V'\tau_m}{2\omega V_0} e^{2\omega t/\tau_m}(1-e^{-2\omega f/V_0\tau_m}) . \quad \text{(B3)}$$

Substituting (4.12) and (4.13) into (B1) and linearizing with respect to ϵ, the integrals in Eq. (B1) can easily be performed. Taking into account the value (4.3) of c_0, we finally obtain after some algebra the eigenvalue equation

$$\sqrt{\omega+1}=\frac{\omega Q-P}{\omega-P} ,$$

with P and Q defined in (4.16) and (4.17).

[1] D. Kessler, J. Koplik, and H. Levine, Adv. Phys. **37**, 255 (1988); W. Kurz and R. Trivedi, Acta Metall. **38**, 1 (1990).
[2] A. Karma and A. Sarkissian, Phys. Rev. E **47**, 513 (1993).
[3] W. van Saarloos and J. D. Weeks, Physica D **12**, 279 (1984).
[4] G. H. Gilmer and H. J. Leamy, in *Laser and Electron Beam Processing of Materials,* edited by C. W. White and P. S. Peercy (Academic, New York, 1980), p. 227; D. A. Kurtze, W. van Saarloos, and J. D. Weeks, Phys. Rev. B **30**, 1398 (1984); D. G. Kurtze, Phys. Rev. Lett. **60**, 1638 (1988).
[5] C. Harloff, Leidsch. Geol. Med. **2**, 99 (1927); E. S. Larsen and J. Irving, J. Am. Miner. **23**, 227 (1938); J. Vance, Am. J. Sci. **260**, 746 (1962).
[6] T. H. Pearce, Can. Mineral. **22**, 383 (1984); T. H. Pearce, J. K. Russell, and I. Wolfson, Am. Mineral. **72**, 1131 (1987); T. H. Pearce and A. H. Clark, Geology **17**, 757 (1989); T. H. Pearce and A. M. Kolisnik, Earth-Sci. Rev. **29**, 9 (1990).
[7] N. Shimizu, Earth-Sci. Rev. **29**, 27 (1990).
[8] T. H. Pearce, Contrib. Mineral Petrol. **97**, 459 (1987).
[9] B. W. D. Yardley, C. A. Rochelle, A. C. Barnociat, and G. E. Lloyd, Mineral. Mag. **55**, 357 (1991).
[10] R. T. Cygan and A. C. Lasaga, Contrib. Mineral. Petrol. **79**, 187 (1982); B. Jamtveit, Am. Mineral. **76**, 1319 (1991).
[11] Y. Wang and E. Merino, Geochim. Cosmochim. Acta **56**, 587 (1992).
[12] A. Putnis, L. Fernandez-Diaz, and M. Prieto, Nature **358**, 743 (1992).
[13] G. Brandeis, C. Jaupart, and C. J. Allègre, J. Geophys. Res. **89**, 10 161 (1984).
[14] C. J. Allègre, A. Provost, and C. Jaupart, Nature **294**, 223 (1981).
[15] C. S. Haase, J. Chadam, D. Feinn, and P. Ortoleva, Science **209**, 272 (1980); P. J. Ortoleva, Earth-Sci. Rev. **29**, 3 (1990).
[16] A. C. Lasaga, Am. J. Sci. **282**, 1264 (1982).
[17] J. W. Rutter and B. Chalmers, Can. J. Phys. **31**, 15 (1953); W. A. Tiller, K. A. Jackson, J. W. Rutter, and B. Chalmers, Acta Metall. **1**, 428 (1953); D. F. Sibley, T. A. Vogel, B. M. Walker, and G. Byerly, Am. J. Sci. **276**, 275 (1976).
[18] R. J. Kirkpatrick, L. Klein, D. R. Uhlmann, and J. F. Hays, J. Geol. Res. **84**, 3671 (1979).
[19] F. Albarede and Y. Bottinga, Geochim. Cosmochim. Acta **36**, 141 (1972).
[20] D. F. Weill, R. Hon, and A. Navrotsky, in *Physics of Magmatic Processes,* edited by R. B. Hargraves (Princeton University Press, Princeton, 1980), p. 49.
[21] R. J. Kirkpatrick, J. Geol. Res. **81**, 2565 (1976); R. J. Kirkpatrick, G. R. Robinson, and J. F. Hays, *ibid.* **81**, 5715 (1976).
[22] G. E. Muncill and A. C. Lasaga, Am. Miner. **72**, 299 (1987).
[23] P. D. Calvert and D. R. Uhlmann, J. Crys. Growth **12**, 291 (1972); for a good review of the growth processes in igneous rocks, see E. Dowty, in *Physics of Magmatic Processes* (Ref. [20]), p. 419.
[24] Y. Bottinga and D. F. Weill, Am. J. Sci. **272**, 438 (1972).
[25] V. G. Smith, W. A. Tiller, and J. W. Rutter, Can. J. Phys. **33**, 723 (1955).
[26] A. D. Fowler (private communication). The estimate is based on typical magma chamber volumes and volcanic eruption rates.
[27] A. D. Fowler (private communication).
[28] S. V. Patankar, *Numerical Heat Transfer and Fluid Flow* (McGraw-Hill, Washington, DC, 1980).
[29] W. Horsthemke and R. Lefever, *Noise-Induced Transitions. Theory and Applications in Physics, Chemistry and Biology* (Springer, Berlin, 1984); *Noise in Non-linear Dynamical Systems,* edited by F. Moss and P. V. E. McClintock (Cambridge University Press, Cambridge, 1988).
[30] A. C. Lasaga, S. M. Richardson, and H. D. Holland, in *Energetics of Geological Processes,* edited by S. K. Saxena and S. Bhattacharji (Springer, New York, 1977), p. 353.